Journal of Glaciology, Vol. 39, No. 133, 1993

The tensile strength of first-year sea ice

J. A. Richter-Menge and K. F. Jones
U.S. Army Cold Regions Research and Engineering Laboratory, Hanover, New Hampshire 03755, U.S.A.

ABSTRACT. We present the results of tests done to determine the tensile behavior of first-year columnar sea ice over a range of temperatures from –20° to –3°C and strain rates of 10^{-5} and 10^{-3} s^{-1}. The temperature of a test specimen was dictated by its in-situ location within the sea-ice sheet; samples located near the top of the sea-ice sheet were tested at the lower temperatures. A tensile load was applied along the cylindrical axes of the test specimens, which were perpendicular to the growth direction of the ice. Results showed that the maximum stress reached during a test was most strongly influenced by temperature, while the failure strain and the modulus were principally affected by the loading rate. A model relating the tensile strength of the ice to its porosity based on temperature-dependent variations in the brine-pocket geometry is evaluated.

INTRODUCTION

Ice is substantially weaker in tension than it is in compression at strain rates greater than 10^{-5} s^{-1} (Mellor, 1983). Tensile stresses are introduced in an ice sheet when it undergoes flexure, as is often the case during full-scale ice–ice or ice–structure interaction events in the Arctic region. In-situ stress measurements (Tucker and Perovich, 1992) indicate that during such events there is a variation in stress through the thickness of the ice sheet associated with flexure and that tensile stresses are not uncommon. Because the ice can withstand relatively high compressive stresses, it follows that under these conditions failure is generally controled by the tensile strength of the ice. It is particularly important, therefore, that a better understanding of the behavior of ice in tension is developed so that its influence can be appropriately considered in engineering-design problems and geophysical models.

Given the difficulty of determining the direct tensile strength of ice, via mechanical-property testing, very few studies have focused on the subject. This is particularly true with respect to saline ice, which has an inherently complex structure. Previous related works discussing the tensile properties of saline ice include those on columnar first-year sea-ice samples by Peyton (1966), Saeki and others (1978) and Dykins (1970), who tested columnar saline samples grown in the laboratory. More recently, work has been done by Kuehn and others (1990) on both natural and laboratory-grown saline ice with a columnar structure.

The data presented in this paper provide information on the tensile behavior of columnar, first-year sea ice at four different temperatures (–20°, –10°, –5° and –3°C) and two strain rates (10^{-3} and 10^{-5} s^{-1}). Specifically described are the maximum tensile stress and corresponding failure strain, and the initial and failure moduli as a function of these test parameters. All of the test specimens were prepared from cylindrical ice cores that had been taken from the horizontal plane of the ice sheet. Through application of a load along the cylindrical axis of the test specimen, a failure plane was created parallel to the long axis of the columnar ice. This corresponds to the orientation of the failure plane expected when the ice sheet experiences flexure due to either bending or buckling (Fig. 1).

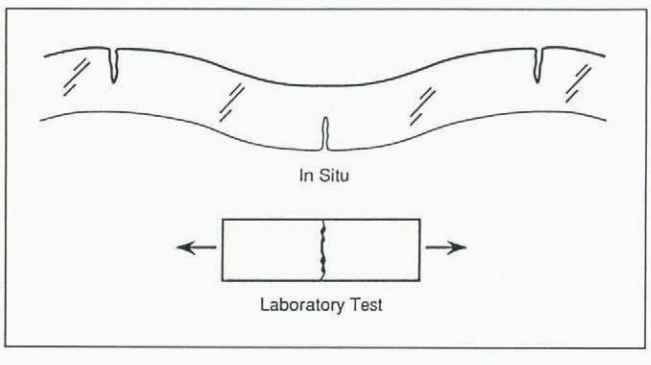

Fig. 1. Sample orientation relative to the failure plane of an ice sheet experiencing a flexural load.

Combining the results from these experiments with observations of the changes in brine-pocket geometry as a function of temperature, we evaluate a model that relates the porosity of the columnar ice to its tensile strength. While never tested for its ability to represent the tensile strength of sea ice, this physically based model was originally suggested in earlier works by Assur (1960) and Weeks and Assur (1967).

ICE DESCRIPTION

Ice samples for the test program were collected during April 1986, when the average daytime air temperature

https://doi.org/10.3189/S0022143000016506 Published online by Cambridge University Press

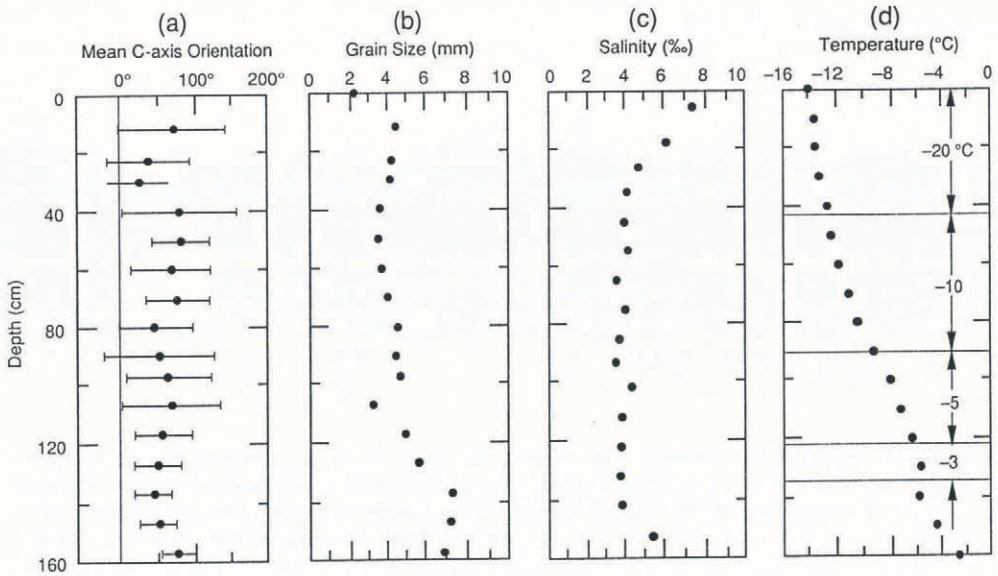

Fig. 2. Profile characteristics of the ice sheet sampled for this test program. Plotted, vs depth, are (a) the mean c-axis orientation relative to magnetic north (0°) and the degree of spread, (b) the average grain-size (mm), (c) the salinity (ppt) and (d) the temperature (°C). The relationship between test temperature and sample depth is also indicated in (d).

was −15°C. The sampling site was established on a 166 cm thick, refrozen lead located in the Alaskan Beaufort Sea, approximately 160 km north of Barter Island. The horizontally oriented samples collected for testing were retrieved using a coring method described by Richter-Menge and others (1986). Briefly, a 30.5 cm diameter vertical core was initially taken from the ice sheet. This ice core was then placed on its side in a drill press equipped with a 10.8 cm diameter hole saw. Samples were taken along the length of the 30.5 cm diameter ice core. Their exact depth and a description of their crystal structure, including an estimate of the *c*-axis orientation, were recorded in the field notebook. The 10.8 cm diameter samples were then packed for shipment back to the laboratory for testing.

Vertical cores taken specifically to evaluate the physical characteristics of the ice in the 50 m^2 sampling area indicated that at a given depth it was uniform with respect to its crystal structure, salinity and temperature. Profiles of the ice summarizing these physical properties are presented in Figure 2. Vertically elongated crystals, characteristic of congelation or columnar ice, extended through the thickness of the ice sheet. Only a very thin layer of granular ice (< 2 cm) was evident at the top of the ice sheet, indicating quiescent conditions during initial ice formation. Plots of crystal orientations on the Schmidt net indicated that, at 12 cm depth, a *c*-axes horizontal orientation was already well established. However, strong azimuthal alignment of the *c*-axis of the ice in the sampling area did not occur until a depth of 117 cm (Fig. 2a).

The average grain-size of the sea-ice crystals, measured perpendicular to their long axes, remained relatively constant through the ice sheet, averaging 0.41 cm between 12 and 117 cm (Fig. 2b). Within each individual crystal there was a sub-structure defined by brine inclusions separated by platelets of pure ice (Fig. 3). Brine inclusions form as sea water freezes because impurities are not easily incorporated into the ice-crystal lattice. Under the unidirectional growth conditions necessary for the development of columnar sea ice, most of the concentrated, highly saline brine is rejected from the ice sheet at the growth front. This process results in the formation of a dendritic ice/water interface. As the ice sheet continues to grow, some of the brine is trapped between the advancing platelets of pure ice. The distribution of the inclusions is a function of the rate of ice growth (Lofgren and Weeks, 1969; Nakawo and Sinha, 1984). Typically, as in the case of the ice we used for testing, the spacing between the layers of the brine pockets varies from 0.5 to 1.0 mm, increasing with depth as the growth rate decreases. A detailed description of sea-ice growth and the process of brine entrapment can be found in Weeks and Ackley (1986).

The salinity of the ice we sampled varied with depth in accordance with observations made by Nakawo and Sinha (1981) on first-year ice sheets. The salinity was

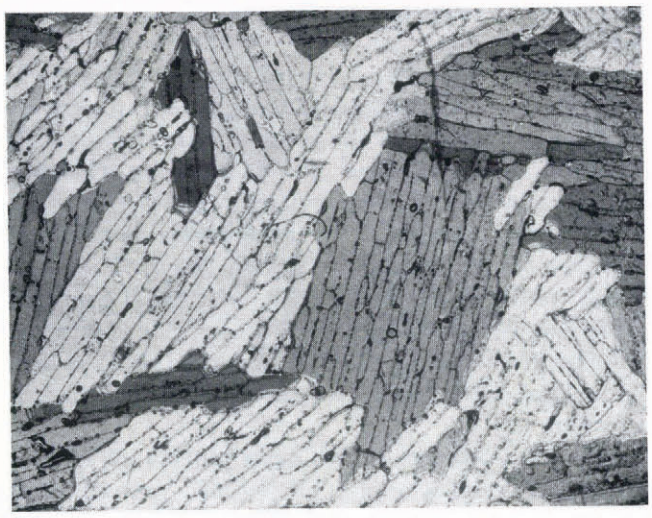

Fig. 3. Crystal sub-structure as seen in a horizontal thin section of columnar sea ice, showing fresh ice platelets separated by brine inclusions (dark areas within individual crystals).

https://doi.org/10.3189/S0022143000016506 Published online by Cambridge University Press

Table 1. Mean (± one standard deviation) salinity, density and porosity of test specimens. Listed alongside the rate is the number of specimens tested at that condition

Temperature	Rate	Salinity	Density	Porosity
°C	s^{-1}	ppt	$Mg\,m^{-3}$	ppt
−20	1E–3 (13)	5.6 ± 1.3	0.922 ± 0.010	18.9 ± 4.2
	1E–5 (12)	5.4 ± 1.1	0.925 ± 0.007	18.1 ± 3.7
−10	1E–3 (17)	4.1 ± 0.3	0.919 ± 0.006	22.5 ± 1.4
	1E–5 (14)	4.1 ± 0.3	0.918 ± 0.005	22.5 ± 1.7
−5	1E–3 (17)	3.5 ± 0.2	0.919 ± 0.004	34.4 ± 2.1
	1E–5 (15)	3.3 ± 0.2	0.916 ± 0.005	33.0 ± 1.8
−3	1E–3 (8)	2.9 ± 0.3	0.913 ± 0.006	57.6 ± 7.0
	1E–5 (7)	3.1 ± 0.2	0.912 ± 0.004	61.5 ± 6.7

relatively high near the top and bottom of the ice sheet. The central part of the ice sheet had a lower salinity, which was nearly constant at 4 ppt (Fig. 2c).

The in-situ temperature profile of the ice sheet (Fig. 2d) was nearly linear, increasing from −12.5°C at a depth of 40 cm to the freezing point of sea water (−1.8°C) at the bottom. Both the salinity and temperature profiles of this ice sheet are typical of late-winter conditions.

The density of each sample was determined by measuring its mass and volume. Its salinity was established after the test by melting the sample once sections had been removed for the crystallographic analysis. The air and brine content (combined to give total porosity) of the samples at the time of testing were calculated using the equations developed by Cox and Weeks (1983). The average density, salinity and porosity of the ice samples at each test condition are given in Table 1.

The average salinity of the samples decreased with an increase in test temperature. This is due, in part, to the drainage of brine that occurs from an ice core during its removal from the parent ice sheet, shipping, storage and warming to test temperature. As discussed in Cox and Weeks (1986), the amount of brine that drains is a function of the temperature history of the ice core. Maximum drainage occurs in samples removed from the warmer, bottom part of the ice sheet. When the brine drains, it leaves behind air-filled inclusions. Hence, this process also results in a decrease in the ice density, which is apparent in Table 1.

As mentioned, a part of this drainage occurs during the 12–24 h warming period needed to establish the test temperature of the ice. Since this was unavoidable, we laid the samples on their sides with the long axes of the columnar crystals vertical while they equilibrated to test temperature. This corresponds to the in-situ orientation of the sample, allowing brine drainage to take place in a natural direction.

After evaluating the error associated with the determination of the brine and air volumes, we found that air-filled voids were a measurable component of the total porosity only in the specimens used for the −3°C tests. In these samples, which had the most variable temperature histories, the air volume accounted for approximately 20% of the total ice porosity. In the remainder of the samples the total porosity was nearly equal to the brine volume. A relatively small air volume is typical of first-year sea ice that remains in situ and has not experienced any significant periods of warming. Consequently, most descriptions of the behavior of first-year sea ice as a function of its porosity only consider the brine volume (e.g. Dykins, 1970). For consistency and completeness, however, total sample porosity rather than brine volume will be used throughout this paper in the reporting and analysis of experimental results.

SAMPLE PREPARATION

Most often, direct tension tests on ice are done using specimens with a reduced central cross-section to ensure failure in the mid-region of the sample (Peyton, 1966; Dykins, 1970; Hawkes and Mellor, 1972; Saeki and others, 1978; Cox and Richter-Menge, 1985; Sinha, 1989). An exception to this is the recent work by Kuehn and others (1990), who tested cylindrical samples of first-year sea ice and laboratory-grown saline ice using an end-capping technique described by Lee (1986). This approach employs Synthane (a phenolic resin reinforced by linen fabric) end caps with jute-backed carpeting epoxied to the face that is frozen to the ice-test specimen. According to the report by Lee, the carpeting increases the bond strength at the ice/end-cap interface and dissipates shear stresses that develop at the interface during application of the load.

We were also able to test successfully cylindrical

https://doi.org/10.3189/S0022143000016506 Published online by Cambridge University Press

samples using an approach that differed from that of Kuehn and others (1990). In early tests, Synthane end caps without carpeting (we could not find a material to duplicate Lee's work) were bonded to the ice according to the procedures suggested by Mellor and others (1984). The end-capped ice-test specimen was attached to the loading machine via a single central thread. Upon application of the tensile load, failure consistently occurred at the ice–end-cap bond. Inspection of the failure plane indicated that localized displacement was occurring in the end cap around the connection, causing an uneven distribution of stresses in the ice near the bond. To prevent this, a steel end plate, bolted around the perimeter of the Synthane end cap (Fig. 4), was incorporated into the loading train. Once this procedure was adopted, failure generally occurred away from the bond interface.

Failures at the ice–end-cap bond that occurred even after incorporation of the steel end plate were caused by bubbles that formed within the fresh-water bond acting as stress risers. To reduce these failures, a significant amount of time was spent developing a technique to produce a fresh-water, bubble-free ice bond. Details of this technique have been described separately by Richter-Menge and others (1993).

Parallel alignment of the end caps was achieved using a method developed by Cole and others (1985) for cored ice samples. We were able to maintain a low deviation from parallelism which averaged 0.052 mm. The maximum deviation permitted in any sample was 0.127 mm. Our initial work indicated that, at height differentials greater than this, failure involved a measurable amount of bending.

The average diameter and length of the test specimens were 10.02 ± 0.03 cm and 25.40 ± 0.02 cm, respectively. Cylindrical specimens were chosen for use in this test program because they could easily be obtained from the ice sheet at depths greater than 1 m and they minimized sample-preparation time. The dimensions of these test specimens do meet or exceed those recommended by Schwarz and others (1981), who suggested that a minimum ratio between sample diameter and grain-size of 15 to 20 be used for tension testing. This guidance was based on the results of tests done on fresh-water granular ice in compression, however, which indicated that at ratios smaller than this the compressive strength was dependent on sample size. While choosing to follow Schwarz and others' recommendations for our tension tests, we recognize that the results from the compression tests may not be directly applicable in determining the dimensions of our tension-test specimens. Significant differences in deformational mechanisms, which could result from a change in loading state and/or ice type, could invalidate the extension. For instance, brine inclusions in sea ice create an inherently flawed material, which may result in a propagation-controlled failure process. In contrast, the failure process in relatively defect-free fresh-water ice is controled by the nucleation of cracks.

Recently, Sinha (1989) presented arguments suggesting that test specimens with a rectangular (prismatic) rather than a circular (cylindrical) cross-section be used when loads are applied to columnar ice in the horizontal plane. He made the very logical point that, given the structural characteristics of columnar ice, prismatic specimens are more compatible with the grain structure in this orientation. Unfortunately, not enough data are available in that paper to make any comparisons with our results that might provide insight into the effects of sample cross-section in tension testing. Obviously, more work needs to be done to define better acceptable sample geometries for tension testing.

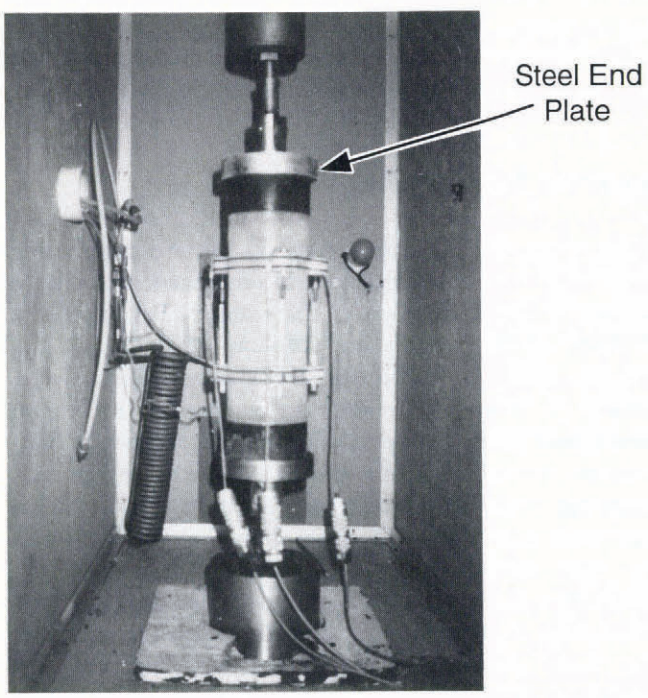

Fig. 4. Instrumented test specimen.

TEST PROCEDURE

All of the tension tests were conducted on a closed-loop electro-hydraulic testing machine. This machine has a high inherent stiffness, with a load frame capacity of 2.2 MN. The 0.11 MN capacity actuator used to apply the tensile load in this test series was equipped with a fast-response, high-flow-rate servo-valve which is capable of providing controled travel speeds of up to $0.42\,\mathrm{m\,s^{-1}}$. Mounted within the frame of the MTS was an environmental chamber that maintained the test temperature to ± 0.2°C. The sample was attached to the testing machine via an assembly that contained a spherical ball joint and pin connections. This system was developed by Currier and Schulson (1982) for tension tests on fresh-water ice samples. A small pre-load (5–15 kPa) was applied to the test specimen in order to seat the loading train.

Sample displacement was measured by three linear variable differential transducers (LVDTs) with a full-range capacity of ± 0.635 mm. The LVDTs were mounted directly on the sample (Fig. 4). They were located 120° apart and measured the displacement over a 14.0 cm section in the center part of of the sample. The individual signals from the LVDTs were averaged and this average was used in the machine's feed-back loop to

control the rate of displacement of the actuator. An evaluation of the individual displacement measurements recorded for each test was made after the test to rule out bending as the failure mode. These observations indicated that extension was occurring at each of the displacement measurement sites and that there was little deviation between the individual readings. The averaged displacement was used in the stress–strain plots for the analysis of the tension data.

An 88% success rate was achieved using these sample-preparation and test techniques. A successful test was defined as one in which the location of the failure plane was within the central 14.0 cm gauge length of the sample. This high level of success is notable for direct tension testing. In particular, it indicates the effectiveness of the end-cap bonding and load-application techniques which were developed for this program.

TEST VARIABLES AND SCHEDULE

A total of 103 constant strain-rate tension tests was performed on the horizontal, columnar first-year sea-ice specimens. The distribution of tests according to experimental variables is given in Table 1. The test temperature of a specimen was chosen, based on its original location in the ice sheet. The range of sample depths that coincided with a specific test temperature is shown in Figure 2d. Assignment of the test strain rate was done to ensure that there was a variation in rate between specimens from the same vertical 30.5 cm core and that there was approximately the same number of 10^{-5} and $10^{-3}\,s^{-1}$ tests at each temperature.

EXPERIMENTAL RESULTS AND DISCUSSION

The results of our tests are presented in Table 2 and compared to those of Dykins (1970) and Kuehn and others (1990) in Figures 5, 6 and 7. For ease of comparison, the points plotted in these figures are the average maximum tensile stress at each test temperature.

Dykins' tests were done on horizontal samples of laboratory-grown columnar saline ice using a screw-driven loading machine operating under constant cross-head velocity. The temperature in his tests ranged from −27° to −4°C and the mean stress rate varied from 0.10 to $0.24\,MPa\,s^{-1}$. Assuming an initial elastic modulus of 5 GPa (based on our results) and predominantly elastic behavior, it is estimated that these tests were done at a strain rate of approximately $3.5 \times 10^{-5}\,s^{-1}$. The diameter of Dykins' test specimens was 4.05 cm. The number of grains per cm^2 in a specimen varied from 2.5 to 0.5. This small diameter relative to the grain-size was necessary due to the constraints of Dykins' test technique and equipment. It should be recognized in considering Dykins' results, however, that this sample size falls far short of the ratio between sample diameter and grain-size of 15–20 recommended by Schwarz and others (1981), which was discussed earlier.

Kuehn's tests were also done on horizontal samples of laboratory-grown columnar saline ice. He tested the ice at a temperature of −10°C and strain rates of 10^{-3} and $10^{-7}\,s^{-1}$ using a sample size, test technique and equipment very similar to ours.

Immediately evident is the strong influence of temperature on the tensile strength (the maximum tensile stress reached during a test) of the saline ice (Fig. 5a). Our results and those of Dykins consistently indicate a decrease in strength with an increase in temperature. This relationship has also been reported by Saeki and others (1978). At any given temperature, however, the maximum tensile stresses measured in our tests are higher than those of both Dykins and Kuehn and others.

This apparent discrepancy between the results is significantly reduced when the strength is replotted as a function of porosity (Fig. 5b). Using this method of

Table 2. Results of the direct tension tests (σ_f = stress at failure, ϵ_f = strain at failure, E_i = initial tangent modulus, E_s = failure modulus). Listed is the mean ± one standard deviation

Temperature °C	*Rate* s^{-1}	σ_f MPa	ϵ_f %	E_i GPa	E_s GPa
−20	1E–3	0.78 ± 0.14	0.012 ± 0.002	7.3 ± 0.8	6.7 ± 0.5
	1E–5	0.73 ± 0.07	0.023 ± 0.004	5.5 ± 0.9	3.3 ± 0.6
−10	1E–3	0.63 ± 0.12	0.010 ± 0.002	7.7 ± 1.8	6.6 ± 0.8
	1E–5	0.56 ± 0.06	0.020 ± 0.006	4.6 ± 0.4	3.0 ± 0.7
−5	1E–3	0.47 ± 0.13	0.008 ± 0.002	6.2 ± 1.2	5.9 ± 1.1
	1E–5	0.45 ± 0.06	0.020 ± 0.006	4.0 ± 0.7	2.4 ± 0.8
−3	1E–3	0.31 ± 0.06	0.008 ± 0.005	5.3 ± 1.3	4.5 ± 1.8
	1E–5	0.21 ± 0.09	0.011 ± 0.009	3.6 ± 1.3	2.6 ± 1.2

https://doi.org/10.3189/S0022143000016506 Published online by Cambridge University Press

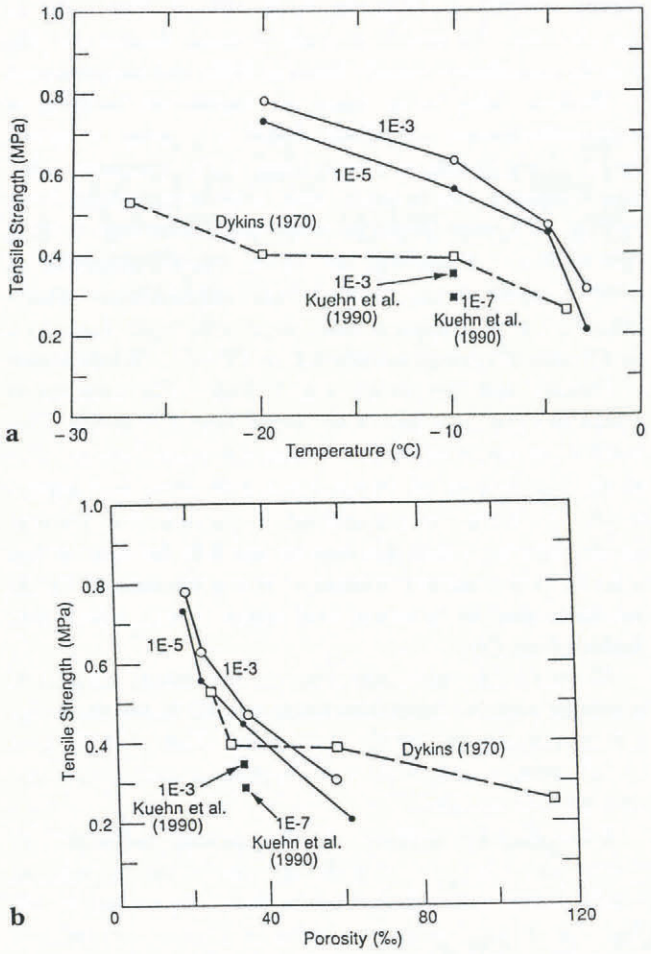

Fig. 5. Maximum tensile stress as a function of (a) temperature and (b) porosity. Plotted are the mean values at each test condition.

comparison, there is very good agreement between the data sets, indicating the importance of porosity in determining the tensile strength of sea ice. The porosity of the ice is related to its temperature. As the temperature of the ice increases, the size of the brine-filled inclusions increases to maintain equilibrium in this three-phase system. This process has a particularly pronounced effect on the integrity of columnar first-year sea ice since the brine inclusions are concentrated in lines between ice platelets (Fig. 3). Observations made by Anderson and Weeks (1958) of the failure plane in a first-year sea-ice beam broken in flexure indicate that when the ice fails in tension it does so by the formation and propagation of cracks along this line of brine inclusions. Dykins (1970) made similar observations. In effect, then, when the brine inclusions increase in size, there is a reduction in the area of ice along the failure plane, causing a decrease in the tensile strength. It is also likely that the relationship among strength, temperature and porosity reflects changes in the stress distribution around the brine inclusions that occur as they vary in size and shape.

Tensile tests done on granular (Schulson and others, 1984) and columnar (Carter and Michel, 1971) fresh-water ice indicate a much less pronounced temperature dependence. This may be a result of a difference in failure mechanisms and/or the fact that fresh-water ice contains only air-filled voids. Unlike brine-filled inclusions in sea ice, there is no marked change in the size or shape of the

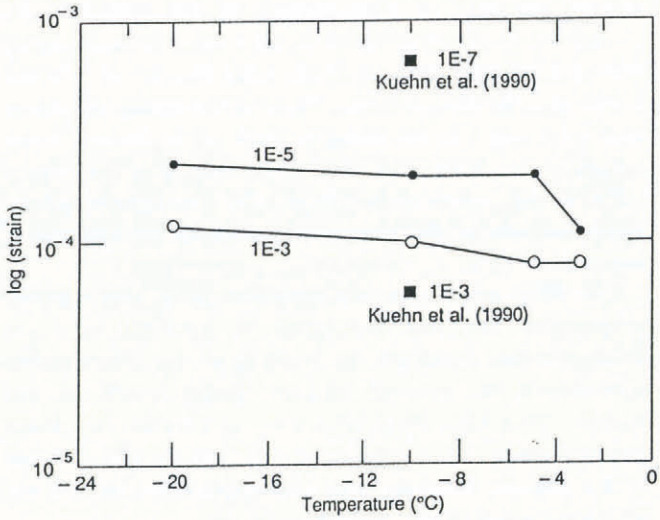

Fig. 6. Strain at the time of maximum stress as a function of temperature.

air bubbles accompanying changes in the ice temperature.

The rate of loading has a much smaller effect on the tensile strength at a given temperature, as can be seen from our data in Figure 5a. It is consistently observed, however, that at each test temperature the tensile strength is higher for the higher strain-rate tests. Similar behavior was reported by Kuehn and others (1990) and in fresh-water ice tension tests by Hawkes and Mellor (1972).

The strain at failure (the strain at maximum stress) is influenced more significantly by changes in the strain rate than temperature (Fig. 6). The failure strain increases with a decrease in the strain rate at all temperatures. Our data indicate only a slight decrease in the strain at failure with an increase in temperature, with the exception of samples tested at 10^{-5} s^{-1} and −3°C, for which the decrease in strain is more pronounced.

The failure modulus (stress divided by strain at maximum stress) is a function of both the strength and failure strain. Consequently, it is influenced by changes in both the temperature and the strain rate. The failure modulus increases with a decrease in temperature and an increase in strain rate (Fig. 7). In Table 2 we see that the

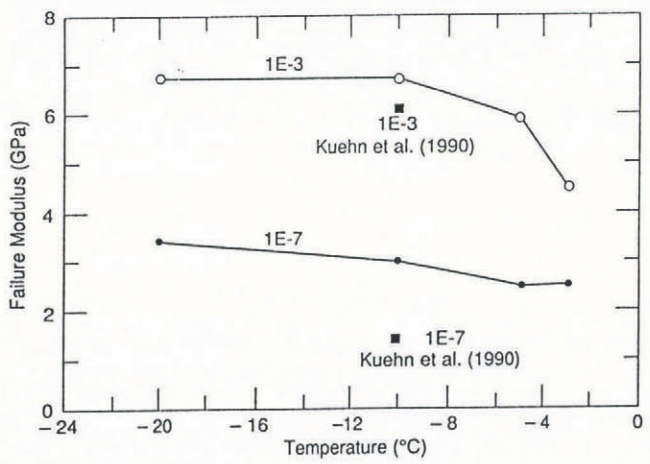

Fig. 7. Failure modulus as a function of temperature.

https://doi.org/10.3189/S0022143000016506 Published online by Cambridge University Press

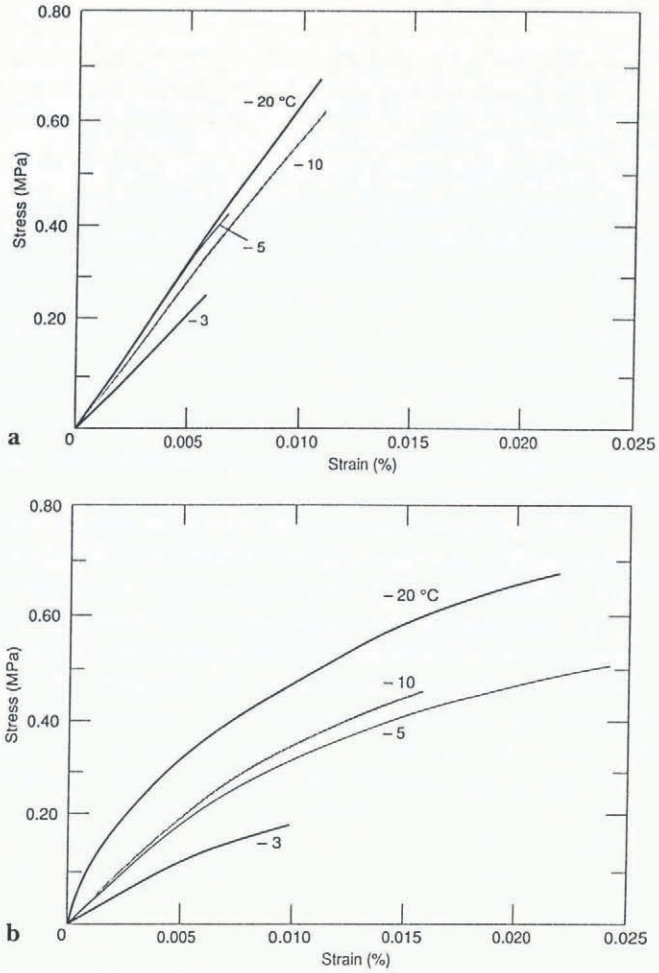

Fig. 8. Representative stress versus strain curves at strain rates of (a) $10^{-3}\,s^{-1}$ and (b) $10^{-5}\,s^{-1}$.

initial tangent modulus (measured by the initial slope of the stress–strain curve) follows these same trends and that it is consistently greater than the failure modulus. Again, these observations are in agreement with those made by Kuehn and others (1990).

The low strains at failure are indicative of the macroscopically brittle behavior observed at all test conditions. Brittle failure is further evidenced by the fact that in all of our tests the strain at failure coincided with the strain at the end of the test. That the initial tangent modulus is consistently higher than the failure modulus suggests, however, that the failure was not a purely elastic phenomenon. The difference between the initial tangent and failure modulus is greater at the lower strain rate, indicating that the non-elastic component of deformation was increasing under these conditions. Typical stress–strain curves from our tests (Fig. 8) confirm this. Again, we point out that even with this difference in the stress–strain behavior of the ice with strain rate, the strength shows little change. The results of Kuehn and others (1990) suggest that this characteristic extends to strain rates of $10^{-7}\,s^{-1}$, where a slight decrease in stress is observed before fracture.

MODELING TENSILE ICE STRENGTH

The results of our tension tests clearly show that changes in the relative volume of the brine inclusions, which occur when the temperature of the ice varies, affect the tensile properties of first-year sea ice. The concentration of the brine inclusions along lines between individual ice platelets and the coincidence of the failure plane with the line of inclusions intensifies these effects. In this section, a model that relates the tensile strength of first-year sea ice to variations in brine-pocket geometry as a function of ice temperature is presented and applied to our results to evaluate its effectiveness. The influence of the distribution of brine inclusions on the tensile strength of first-year sea ice has been considered extensively by Anderson and Weeks (1958), Assur (1960) and Weeks and Assur (1967). To explain this relationship, Assur (1960) introduced a simplified geometric model, representing the brine inclusions between the ice platelets as regularly spaced cylinders whose dimensions change with temperature (Fig. 9). Using this model and available experimental results, Assur (1960) and Weeks and Assur (1967, 1969) then suggested that the tensile strength of first-year sea ice, σ_t, could be related to ψ, the relative reduction in the area of the failure plane (the yz-plane in Figure 9) as follows:

$$\frac{\sigma_t}{\sigma_0} = 1 - \psi \qquad (1)$$

where σ_0 is the strength of a hypothetical sea ice that has no inclusions but maintains the same crystal substructure. Recognizing that ψ is a function of the total ice porosity and further assuming that the porosity of first-year sea ice is equal to the volume of brine, ν_b, they rewrote Equation (1) as

$$\frac{\sigma_t}{\sigma_0} = 1 - \left(\frac{\nu_b}{\nu_0}\right)^k \qquad (2)$$

where k is a parameter that relates the changes in porosity to the dimensional changes in brine-pocket geometry that occur as a function of temperature and ν_0 represents the brine volume associated with an ice structure that cannot sustain load. We suggest that for columnar ice ν_0 is

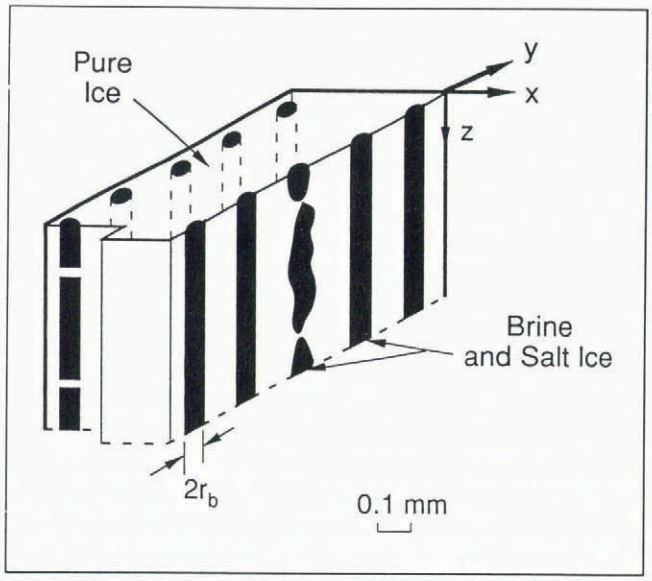

Fig. 9. Idealized diagram of the shape of brine inclusions in sea ice (Assur, 1960).

https://doi.org/10.3189/S0022143000016506 Published online by Cambridge University Press

equivalent to the brine volume of the skeletal layer where the dendritic platelets of ice are no longer laterally connected and, hence, cause the ice to lose its structural integrity.

Measurements made by Anderson and Weeks (1958) using microphotographs to document the variations in brine-pocket geometry with temperature can be used to define k and approximate ν_0. As we have discussed, the brine inclusions become larger to maintain phase equilibrium as the temperature of the ice increases. Anderson and Weeks found that, as the ice warms, the brine inclusions, which are circular cylinders, increase in diameter up to approximately 0.07 mm. Further growth of the brine inclusions is then limited to the y-direction, parallel to the platelets, and the circular cross-section becomes elliptical. Growth continues in this direction until the brine inclusions coalesce, forming the skeletal or dendritic layer that characterizes the bottom of a columnar sea-ice sheet. Anderson and Weeks estimated the porosity of the skeletal layer as approximately 150 ppt. Similar observations have been made by Langhorne and others (1980).

At the lower temperatures then, geometric similarity is preserved in the xy-plane as the ice warms, the porosity increases and the brine inclusions increase in diameter. Since the porosity is proportional to r_b^2, where r_b is the cylinder radius, the decrease in the area of ice in the failure plane is proportional to $\nu_b^{\frac{1}{2}}$ so $k = \frac{1}{2}$. At higher temperatures, the porosity increase is associated with brine-inclusion growth parallel to the platelets, so the decrease in the area of ice in the failure plane is proportional to ν_b and $k = 1$. These two processes are represented in the ice-strength model

$$\frac{\sigma_t}{\sigma_0} = \left[1 - \left(\frac{\nu_b}{\nu_0}\right)^{\frac{1}{2}}\right]^2. \tag{3}$$

This expression can be expanded to

$$\frac{\sigma_t}{\sigma_0} = 1 - 2\left(\frac{\nu_b}{\nu_0}\right)^{\frac{1}{2}} + \frac{\nu_b}{\nu_0} \tag{4}$$

to show explicitly the dependence of σ_t on ν_b and ν_b^2. The relationship in Equation (3) can be presented as a straight line with ordinate $\sigma_t^{\frac{1}{2}}$, abscissa $\nu_b^{\frac{1}{2}}$, and x-intercept $\nu_0^{\frac{1}{2}}$.

While Weeks and Assur originally presented the ice-strength model given in Equation (4), its effectiveness in describing the results of tension-test data was not evaluated. Instead, a relationship expressing the tensile strength of first-year sea ice as a function of the square root of the brine volume was adopted. Assur (1960) did point out the potential weakness of the $\sigma_t - (\nu_b)^{\frac{1}{2}}$ model at higher temperatures based on his observation that the tensile strength did not approach zero as a linear function of $\nu_b^{\frac{1}{2}}$. Dykins (1970) also analyzed his tension data using the $\sigma_t - (\nu_b)^{\frac{1}{2}}$ model, adding support to this approach.

We decided to evaluate further the $(\sigma_t)^{\frac{1}{2}} - (\nu_b)^{\frac{1}{2}}$ ice-strength model because we felt that its physical basis made it a stronger candidate for incorporation into larger-scale models, for example, finite-element models of ice-sheet failure. It was decided that the two models should be compared by performing least-square regression analyses on our own and Dykins' (1970) test data. Individual data points were used for each regression analysis rather than the mean at a given test condition to provide a more statistically satisfying evaluation. Dykins' results on brackish ice samples were not included because we believed that the structural characteristics of this ice type might differ from those of ice grown at salinities representative of standard sea water. In all cases, the total porosity rather than the brine volume of the samples was used in the analysis, since both data sets involved ice that had been removed from an ice sheet. As we discussed earlier, the process of removing ice from its in-situ state and preparing samples for testing can result in the drainage of some of the brine inclusions, leaving air-filled voids. Calculation of porosity was done for each of Dykins' samples using his reported measurements of density and salinity.

In the regression analysis of our data, the square root of the porosity was chosen as the variable to be fitted for both models. This reflected our higher degree of certainty in the accuracy of the maximum stress measurement relative to the calculation of porosity using the mass and volume of the test specimens. An analysis of the dimensional characteristics of our core samples indicated that significant variations in the diameter of the sample occurred along its length, affecting the accuracy of the determination of volume and, therefore, porosity.

Based on the information provided in Dykins' report, we were not confident in our ability to decide if his strength measurement or porosity calculation was less accurate and should be fitted. Therefore, a technique presented by York (1966) was applied that minimizes the sum of the squares of the perpendicular distances of the data points to the best-fit line. This approach determines a "reduced major axis" by assuming that the x and y errors in the data are proportional to the x and y standard deviations, respectively.

The results of the analysis are summarized in Table 3 and shown graphically in Figures 10 and 11. Comparison

Table 3. Results from linear least-squares regression analyses to determine the relationship between the tensile strength of sea ice and its porosity. Assuming: $x = a_1 y + a_2$

Model	$\dot{\epsilon}$	a_1	a_2	r^2	ν_0
	s^{-1}				ppt
$y = (\sigma_t)^{\frac{1}{2}}$	1E–3	–6.76	10.54	0.63	111
$x = (\nu_b)^{\frac{1}{2}}$	1E–5	–7.83	11.08	0.75	123
	* 3.5E–5	–13.51	11.19	0.17	170
$y = \sigma_t$	1E–3	–4.40	8.03	0.60	64
$x = (\nu_b)^{\frac{1}{2}}$	1E–5	–5.92	8.62	0.75	74
	* 3.5E–5	–8.81	9.75	0.16	95

* Based on tension-test data presented by Dykins (1970).

https://doi.org/10.3189/S0022143000016506 Published online by Cambridge University Press

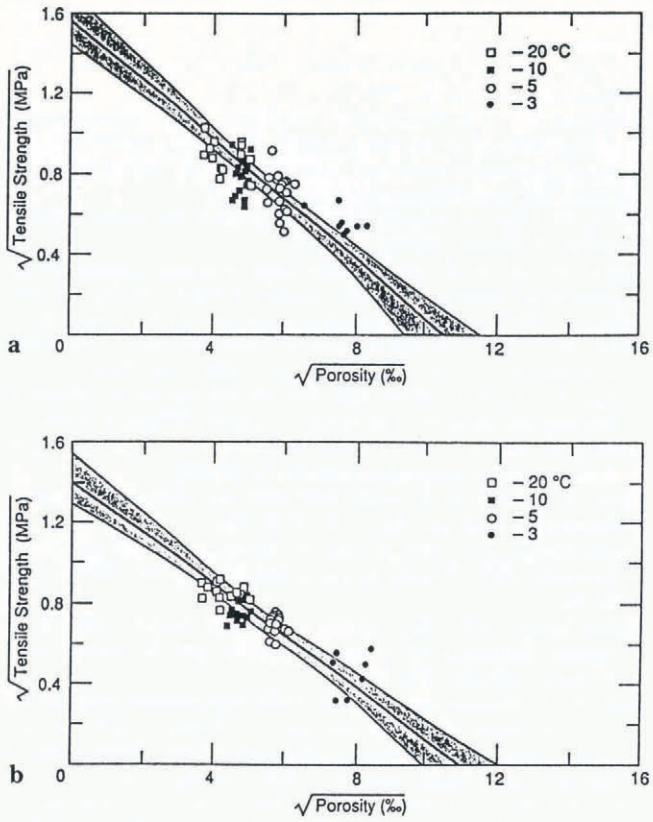

Fig. 10. Least-squares regression analysis of tension data using $(\sigma_t)^{\frac{1}{2}} - (\nu_b)^{\frac{1}{2}}$ model at strain rates of (a) $10^{-3}\,s^{-1}$ and (b) $10^{-5}\,s^{-1}$. The shaded area represents the 95% confidence interval.

of r^2, the square of the correlation coefficients, of the $(\sigma_t)^{\frac{1}{2}} - (\nu_b)^{\frac{1}{2}}$ and the $\sigma_t - (\nu_b)^{\frac{1}{2}}$ models in each case indicates that the quality of the fit is similar for both models. The r^2 for Dykins' data is much lower than for our experiments, reflecting a much greater degree of scatter in his strength measurements at each temperature. This scatter is probably associated with the relatively small ratio of sample diameter to grain-size in his test specimens. The r^2 for our data of 0.63 and 0.74 reflect the inherent variability in the physical properties of ice and its effect on the tensile strength.

To compare the models further, the regression lines were extended to find the x-intercept. This was done

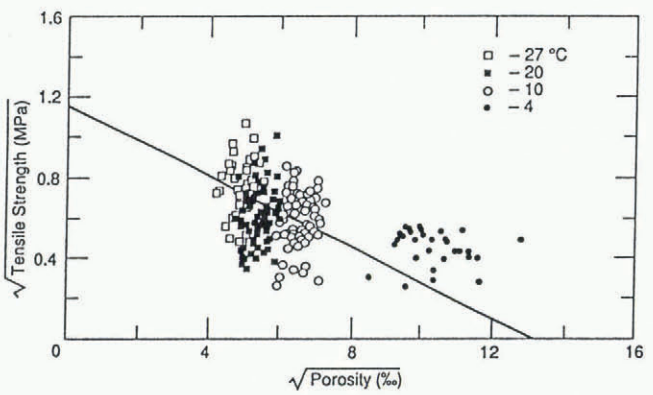

Fig. 11. Linear least-squares regression analysis using a reduced major axis (York, 1966) of Dykins' (1970) tension data.

recognizing that ideally any interpretation of the results made from an extrapolation should be confirmed by further testing. In both cases, the intercept represents the value predicted for ν_0, the porosity associated with an ice structure that cannot sustain load. We have suggested that for columnar ice this porosity is equivalent to the porosity of the skeletal layer, estimated to be approximately 150 ppt. The results of this comparison indicate that the $(\sigma_t)^{\frac{1}{2}} - (\nu_b)^{\frac{1}{2}}$ model consistently gives a more reasonable value for ν_0. The 95% confidence intervals, included in Figure 10a and b, show that this model predicts $\nu_0 = 111 \pm 11$ and $\nu_0 = 123 \pm 11$ for the 10^{-3} and $10^{-5}\,s^{-1}$ strain rates, respectively. As discussed by Assur (1960), the $\sigma_t - (\nu_b)^{\frac{1}{2}}$ model gives a ν_0 that is much lower than that estimated by using physical measurements. This is due to the fact that the $\sigma_t - (\nu_b)^{\frac{1}{2}}$ model does not represent the changes that occur in the brine inclusions at higher temperatures.

The y-intercept was not considered in the evaluation of these models because it represents zero-porosity ice with the same structure as sea ice, which does not exist.

SUMMARY AND CONCLUSIONS

The tensile strength of first-year ice is extremely dependent on temperature due, in great part, to the influence of temperature on brine volume. As the temperature increases, the brine volume (and hence porosity) of the ice increases and causes a decrease in the tensile strength of the ice. This dependency is intensified because the brine inclusions are concentrated along lines that coincide with the plane of failure. While the rate of loading has a much less dramatic effect on the strength of the ice, it does significantly influence the failure strain and modulus. As the loading rate increases from 10^{-5} to $10^{-3}\,s^{-1}$, the failure strain decreases and the modulus increases. This behavior is reflected in the stress–strain plots of our data where, as the rate increases, the linearity of the plots becomes more pronounced. Taken together, these characteristic behaviors indicate that while the failure of the ice was observed to be macroscopically brittle at all test conditions, the process is not purely elastic. Instead, as the temperature increases and the loading rate decreases, the non-elastic component of deformation increases.

Using the results of our tests, we evaluated and compared two models that relate the tensile strength of the sea ice to its porosity. Both were originally suggested by Weeks and Assur (1967). One, which is commonly used in the analysis of tension data, describes the strength as a function of the square root of the porosity. The other relates the square root of the strength to the square root of the porosity. The former was adopted by Weeks and Assur based on experimental results available at the time, even though it had been suggested in Assur (1960) that the tensile strength did not approach zero linearly with the square root of porosity. Weeks and Assur did recognize the advantage of the $(\sigma_t)^{\frac{1}{2}} - (\nu_b)^{\frac{1}{2}}$ model: that it provides a more accurate representation of the geometric changes that occur in the brine inclusions as the temperature of the ice changes. However, it was never evaluated.

https://doi.org/10.3189/S0022143000016506 Published online by Cambridge University Press

We made the comparison of the two models using a least-squares regression analysis. While both models provided comparable fits to the data, the $(\sigma_t)^{\frac{1}{2}} - (\nu_b)^{\frac{1}{2}}$ model gives a more reasonable estimate of the porosity of the skeletal layer because it accurately describes the changes that occur in the brine inclusions at higher temperatures. The capability of this model to represent the tensile strength at the under side of the ice sheet makes it particularly useful for predicting the flexural failure of an ice sheet.

ACKNOWLEDGEMENTS

The authors appreciate the efforts of G. Durell, N. Perron and B. Elder in preparing and testing the ice samples and the assistance provided by Dr G. Cox in initiating this project and assisting with the data-analysis techniques. They also thank Dr D. Cole for his thorough and insightful review of the manuscript. The test program was sponsored by David Taylor Navy Ship Research and Development Center. Additional funds for the development of the model were provided by the U.S. Office of Naval Research under contract #N000149MP2.

REFERENCES

Anderson, D. L. and W. F. Weeks. 1958. A theoretical analysis of sea-ice strength. *Trans. Am. Geophys. Union*, **39**(4), 632–640.

Assur, A. 1960. Composition of sea ice and its tensile strength. *CRREL Res. Rep.* 44.

Carter, D. and B. Michel. 1971. *Lois et mécanismes de l'apparente rupture de la glace de rivière et de lac.* Québec, Université Laval. Department of Civil Engineering. (Report S-22.)

Cole, D. M., L. D. Gould and W. D. Burch. 1985. A system for mounting end caps on ice specimens. *J. Glaciol.*, **31**(109), 362–365.

Cox, G. F. N. and J. A. Richter-Menge. 1985. Tensile strength of multi-year pressure ridge sea ice samples. *ASME Journal of Energy Resources Technology*, **107**(3), 375–380.

Cox, G. F. N. and W. F. Weeks. 1983. Equations for determining the gas and brine volumes in sea ice samples. *J. Glaciol.*, **29**(102), 306–316.

Cox, G. F. N. and W. F. Weeks. 1986. Changes in the salinity and porosity of sea-ice samples during shipping and storage. *J. Glaciol.*, **32**(112), 371–375.

Currier, J. H. and E. M. Schulson. 1982. The tensile strength of ice as a function of grain size. *Acta Metall.*, **30**(8), 1511–1514.

Dykins, J. E. 1970. *Ice engineering: tensile properties of sea ice grown in a confined system.* Port Hueneme, CA, Naval Civil Engineering Laboratory. (NCEL Technical Report R680.)

Hawkes, I. and M. Mellor. 1972. Deformation and fracture of ice under uniaxial stress. *J. Glaciol.*, **11**(61), 103–131.

Kuehn, G. A., R. W. Lee, W. A. Nixon and E. M. Schulson. 1990. The structure and tensile behavior of first-year sea ice and laboratory-grown saline ice. *ASME Journal of Offshore Mechanics and Arctic Engineering*, **112**(4), 357–363.

Langhorne, P. J., J. R. Rossiter and T. E. Keliher. 1980. *Remote estimation of the properties of sea ice, ice core analysis, Beaufort Sea, March 1979.* St. John's, Memorial University of Newfoundland. Centre for Cold Ocean Resources Engineering. (C-Core 80-7.)

Lee, R. W. 1986. A procedure for testing cored ice under uniaxial tension. *J. Glaciol.*, **32**(112), 540–541.

Lofgren, G. and W. F. Weeks. 1969. Effect of growth parameters on substructure spacing in NaCl ice crystals. *J. Glaciol.*, **8**(52), 153–164.

Mellor, M. 1983. Mechanical behavior of sea ice. *CRREL Monogr.* 83-1.

Mellor, M., G. F. N. Cox and H. Bosworth. 1984. Mechanical properties of multi-year sea ice: testing techniques. *CRREL Rep.* 84-8.

Nakawo, M. and N. K. Sinha. 1981. Growth rate and salinity profile of first-year sea ice in the High Arctic. *J. Glaciol.*, **27**(96), 315–330.

Nakawo, M. and N. K. Sinha. 1984. A note on brine layer spacing of first-year sea ice. *Atmosphere-Ocean*, **22**(2), 193–206.

Peyton, H. R. 1966. *Sea ice strength.* Fairbanks, AK, University of Alaska. Geophysical Institute. (Report UAG-R-182.)

Richter-Menge, J. A., G. F. N. Cox, N. Perron, G. Durell and H. W. Bosworth. 1986. Triaxial testing of first-year sea ice. *CRREL Rep.* 86–16.

Richter-Menge, J. A., K. J. Claffey and M. R. Walsh. 1993. End-capping procedure for cored ice samples used in tension tests. *J. Glaciol.*, **39**(133), 698–700.

Saeki, H., T. Nomura and A. Ozaki. 1978. Experimental study on the testing methods of strength and mechanical properties for sea ice. *IAHR. International Association for Hydraulic Research. Symposium on Ice Problems, Luleå, Sweden, August 7–9, 1978. Proceedings. Part 1*, 135–149.

Schulson, E. M., P. N. Lim and R. W. Lee. 1984. A brittle to ductile transition in ice under tension. *Philos. Mag., Ser. A*, **49**(3), 353–363.

Schwarz, J. *and 7 others.* 1981. Standardized testing methods for measuring the mechanical properties of ice. *Cold Reg. Sci. Technol.*, **4**(3), 245–253.

Sinha, N. K. 1989. Closed-loop controlled tensile strength testing method for multi-year sea ice. *In* Sinha, N. K., D. S. Sodhi and J. S. Chung, *eds. Proceedings of the Eighth International Conference on Offshore Mechanics and Arctic Engineering, The Hague, The Netherlands, March 19–23, 1989. Vol. 4. Arctic and polar technology.* New York, American Society of Mechanical Engineers, 1–6.

Tucker, W. B., III and D. K. Perovich. 1992. Stress measurements in drifting pack ice. *Cold Reg. Sci. Technol.*, **20**(2), 119–139.

York, D. 1966. Least-squares fitting of a straight line. *Can. J. Phys.*, **44**, 1079–1086.

Weeks, W. F. and S. F. Ackley. 1986. The growth, structure, and properties of sea ice. *In* Untersteiner, N., *ed. The geophysics of sea ice.* New York, Plenum Press, 9–164.

Weeks, W. F. and A. Assur. 1967. Mechanical properties of sea ice. *CRREL Monogr.* II-C3.

Weeks, W. F. and A. Assur. 1969. Fracture of lake and sea ice. *CRREL Res. Rep.* 269.

The accuracy of references in the text and in this list is the responsibility of the authors, to whom queries should be addressed.

MS received 2 March 1992 and in revised form 6 April 1993